

Calculation of Energy Band Diagram of a Photoelectrochemical Water Splitting Cell

Peter Cendula,^{*,†} S. David Tilley,[‡] Sixto Gimenez,[¶] Juan Bisquert,[¶] Matthias Schmid,[†] Michael Grätzel,[‡] and Jürgen O. Schumacher[†]

*Institute of Computational Physics, Zurich University of Applied Sciences (ZHAW),
Wildbachstrasse 21, 8401 Winterthur, Switzerland, Laboratory of Photonics and Interfaces, Ecole
Polytechnique Fédérale de Lausanne, EPFL-SB-ISIC-LPI, Station 6, 1015 Lausanne,
Switzerland, and Photovoltaics and Optoelectronic Devices Group, Departament of Physics,
University Jaume I, 12071 Castellon, Spain*

E-mail: cend@zhaw.ch

^{*}To whom correspondence should be addressed

[†]Zurich University of Applied Sciences

[‡]Ecole Polytechnique Fédérale de Lausanne

[¶]University Jaume I

Abstract

A physical model is presented for a semiconductor electrode of a photoelectrochemical (PEC) cell, accounting for the potential drop in the Helmholtz layer. Hence both band edge pinning and unpinning are naturally included in our description. The model is based on the continuity equations for charge carriers and direct charge transfer from the energy bands to the electrolyte. A quantitative calculation of the position of the energy bands and the variation of the quasi-Fermi levels in the semiconductor with respect to the water reduction and oxidation potentials is presented. Calculated current-voltage curves are compared with established analytical models and measurement. Our model calculations are suitable to enhance understanding and improve properties of semiconductors for photoelectrochemical water splitting.

Introduction Research on hydrogen production by photoelectrochemical (PEC) cells is propelled by the worldwide quest for capturing, storing and using solar energy instead of decreasing fossil energy reserves. Hydrogen is widely considered as a key solar fuel of the future.¹ Hydrogen is also part of power to gas conversion systems developed to resolve intermittency in the wind and solar energy production.² Although a PEC/photovoltaic cell with 12.4% efficiency was demonstrated with GaInP₂/GaAs,³ decreasing its cost and increasing its lifetime are still under way. An alternative approach often pursued is to use abundant and cheap metal oxides as a viable class of semiconductor materials for PEC electrodes.⁴⁻⁶ However, their recombination losses, charge carrier conduction and water oxidation properties need to be understood and optimized both by measurement and numerical simulation.⁷

Several approaches for a mathematical analysis of semiconductor electrodes can be found in the literature, including analytical^{8,9} and numerical models^{10,11} of PEC cells. An extensive numerical study of PEC behavior of Si and GaP nanowires was recently conducted with commercial software.¹² Since surface states play a major role for many semiconductors, corresponding models were also developed to analyze their effect on electrochemical measurements.¹³⁻¹⁵ On the PEC system level, models of the coupled charge and species conservation, fluid flow and electrochemical reactions were recently developed.^{16,17} The latter studies revealed how PEC systems should

be designed with minimal resistive losses and low crossover of hydrogen and oxygen by use of a non-permeable separator.

Almost every publication on PEC cells features a schematic energy band diagram of a PEC cell, mostly sketched by hand from basic physical understanding described in textbooks on electrochemistry.^{7,18,19} Although such sketches might be qualitatively correct, numerical calculations of the charge carrier transport might reveal additional features not captured by the sketches. We are aware that the development of numerical calculations is frequently hindered by the complicated physical processes in the actual materials and lack of measurements of parameter values for these processes.²⁰ In spite of these obstacles, we think that the recent advent of user-friendly numerical software and advanced measurement techniques could fill the gap between experimental and numerical approaches if experimentally validated models are developed.

Model In this work, we present calculation of an energy band diagram of a PEC electrode from a physical model with clearly formulated assumptions.²¹ The model is based on charge carrier continuity equations with direct charge transfer from the valence or conduction band to the electrolyte. We consider a PEC cell consisting of an n-type semiconductor with bandgap energy E_g , and an electrolyte which can easily accept a single electron or hole (such as H_2O_2 ²² or $[\text{Fe}(\text{CN})_6]^{3-/4-}$ ²³). Charge transfer occurs across the semiconductor/electrolyte interface until an equilibrium charge distribution is reached and the equilibrium Fermi level in the semiconductor E_{F0} becomes equal to the redox Fermi level E_{redox}

$$E_{F0} = E_{redox}. \quad (1)$$

We reserve subscript 0 for equilibrium values in the dark in the following. To derive our model, we use and repeat some of the general definitions introduced in our previous work²⁴ shown in 1. Note that we use notation of subscript *sc* for semiconductor, *s* for surface quantity, *b* for a bulk semiconductor quantity (where electrons and hole remain at equilibrium in the dark).

Bulk equilibrium properties of the isolated semiconductor are denoted with a subscript 0*i*. The bulk of the semiconductor is electrically neutral, hence the concentration of electrons in the bulk

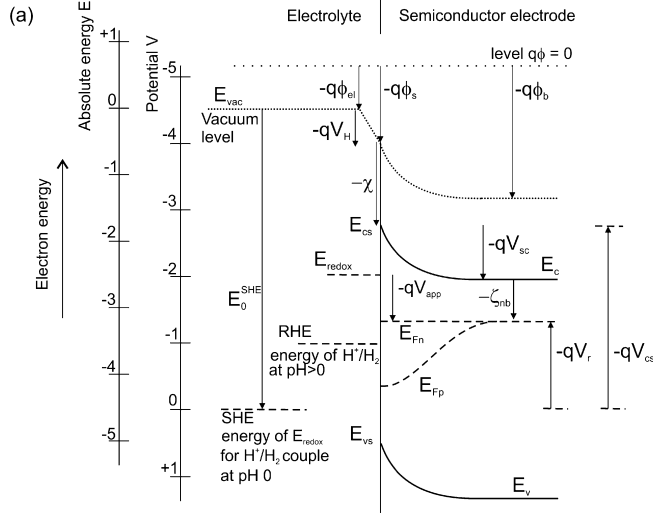


Figure 1: Scheme of a n-type semiconductor electrode, with electron energy indicated in the absolute energy scale (with respect to vacuum level), and potentials in the electrochemical scale, with respect to SHE. Reprinted with permission of ACS.

n_{0i} must be equal to the number of fully ionized donors N_D , $n_{0i} = N_D$. Thus, the concentration of holes is $p_{0i} = n_i^2/n_{0i}$, where n_i denotes intrinsic carrier concentration. An isolated unbiased semiconductor before contact to an electrolyte has a conduction band edge $E_{c,0i}$ and a Fermi level $E_{F,0i}$ related to the vacuum level E_{vac} and electron affinity χ by

$$E_{c,0i} = E_{vac} - \chi, \quad (2)$$

$$E_{F,0i} = E_{c,0i} - \zeta_{nb}, \quad (3)$$

$$\zeta_{nb} = k_B T \ln \left(\frac{N_C}{n_{0i}} \right), \quad (4)$$

where k_B is the Boltzmann constant, T is the temperature, q is the elementary charge and N_C the effective density of states in the conduction band, and ζ_{nb} is the distance of the conduction band edge to Fermi level. In the following, we use $E_{vac}=0$ eV as usual. The potential drop in the Helmholtz layer in the dark V_H is calculated from the local vacuum level (LVL) at the surface of the semiconductor ($-q\phi_s$) and LVL of the electrolyte ($-q\phi_{el}$), ¹,

$$-qV_H = -q\phi_s - (-q\phi_{el}). \quad (5)$$

Note that the potential drop in the Helmholtz layer can be a different value at flatband situation (denoted V_H^{fb}) than at other measurable voltage (denoted V_H). We measure the voltage V_r of the semiconductor electrode with respect to a reference electrode, which means the difference of the Fermi level of electrons in the semiconductor back contact $E_{Fn,b}$ and Fermi level of the reference electrode E_0^{SHE}

$$V_r = -\frac{E_{Fn,b} - E_0^{SHE}}{q}. \quad (6)$$

In this article, we use both the Standard Hydrogen Electrode (SHE) energy and Reversible Hydrogen Electrode (RHE) as reference electrodes and scale of energy. Measured voltage with respect to the SHE is denoted V_r (without subscript SHE) and measurable voltage with respect to the RHE $V_{r,RHE}$ with

$$V_{r,RHE} = V_r + 2.3V_{th} \cdot pH, \quad (7)$$

where $V_{th} = \frac{k_B T}{q}$ is thermal voltage and pH denotes pH value of the solution. We draw attention to the fact that negative bias versus RHE brings the energy closer to the vacuum level E_{vac} . The position of the electron Fermi level at the semiconductor back contact is calculated as (see 1)

$$E_{Fn,b} = -qV_H - \chi - qV_{sc} - \zeta_{nb}, \quad (8)$$

where V_{sc} denotes the potential drop in the semiconductor. What is usually reported in the literature is the value of flatband potential, which is the measurable voltage when the bands are flat ($V_{sc} = 0$)

$$V_{fb} = V_r|_{V_{sc}=0} = \frac{E_0^{SHE} + \chi + \zeta_{nb}}{q} + V_H^{fb}. \quad (9)$$

The value of V_H^{fb} is often not known as it depends on the surface conditions of the semiconductor in the electrolyte. For this article, we know values of V_{fb} and χ and determine V_H^{fb} from the last equation. The potential drop in the semiconductor V_{sc} can be expressed from 1 as

$$-qV_{sc} = -q\phi_b - (-q\phi_s). \quad (10)$$

Then from eqs. ??, ??, ?? follows

$$V_{sc} = V_r - V_{fb} - (V_H - V_H^{fb}). \quad (11)$$

The second option is to refer the voltage to the equilibrium of semiconductor-electrolyte interface (SEI) and this value is denoted V_{app} ²⁴

$$V_{app} = -\frac{E_{Fn,b} - E_{redox}}{q}, \quad (12)$$

$$V_{app} = V_{sc} - V_{bi} + V_H - V_{H0}, \quad (13)$$

where built-in voltage is denoted V_{bi} and potential drop across the Helmholtz layer in dark equilibrium V_{H0} . Equilibrium of SEI means $V_{app} = 0$ V.

On the semiconductor side of the junction, the electrostatic potential ϕ is obtained by solving Poisson's equation¹⁹

$$\frac{d^2\phi}{dx^2} = -\frac{q(N_D - n(x) + p(x))}{\epsilon_0\epsilon_r}, \quad (14)$$

where ϵ_0 is the permittivity of vacuum, ϵ_r is the relative permittivity of the semiconductor, N_D is the concentration of fully ionized donors, $n(x)$ is the concentration of free electrons and $p(x)$ is the concentration of free holes ($p(x) \ll n(x)$ for n-type semiconductor in the dark). We can write for the conduction and the valence band edge energies E_c and E_v in the electrostatic potential $\phi(x)$

$$E_c(x) = -\chi - q(\phi(x) - \phi_{el}), \quad (15)$$

$$E_v(x) = E_c(x) - E_g.$$

The band edge pinning (constant value of $E_c(0)$ and $E_v(0)$) is present if $V_H = V_H^{fb}$ for any measurable voltage (assumed in the following), otherwise the band edges become unpinned.

A simple approximation to solve Poisson's equation, Eq. ??, is to assume that the total space charge is uniformly distributed inside the space charge region (SCR) of width w (also called deple-

tion region approximation)

$$w = \sqrt{\frac{2\epsilon_0\epsilon_r}{eN_D} |V_{sc}|}. \quad (16)$$

The boundary conditions for the electrostatic potential ϕ follow directly from the definitions on 1

$$\phi(0) = \phi_s, \quad (17)$$

$$\phi(w) = \phi_b. \quad (18)$$

The concentration of free electrons and holes in the dark $n_{dark}(x)$ and $p_{dark}(x)$ can be written as

$$n_{dark}(x) = n_{0i} \exp^{\frac{\phi(x)-\phi_b}{V_{th}}}, \quad (19)$$

$$p_{dark}(x) = p_{0i} \exp^{\frac{-\phi(x)+\phi_b}{V_{th}}}. \quad (20)$$

The value of electrostatic potential in the semiconductor bulk ϕ_b appears in the above expressions because we have made general definition of electrostatic potential including the potential drop in the Helmholtz layer. Therefore, ϕ_b is not zero unlike recent textbook definition.⁷ The approximate solution of Poisson's eq. ϕ_a is then

$$\begin{aligned} \phi_a(x) &= \phi_b - \text{sign}(V_{sc}) \frac{qN_D}{2\epsilon_0\epsilon_r} (w-x)^2, & 0 < x < w \\ \phi_a(x) &= \phi_b, & w < x < d. \end{aligned} \quad (21)$$

When the measurable voltage V_r is positive of the flatband potential V_{fb} , the n-type semiconductor is in the depletion regime. When the measurable voltage is negative of the flatband potential, the semiconductor is in the accumulation regime (due to the sign of V_{sc}).

Upon illumination, we assume low-injection conditions with the number of photogenerated electrons lower than the donor concentration. Thus electron concentration is roughly equal to the dark electron concentration $n(x) = n_{dark}(x)$. The hole continuity equation is solved to obtain free

hole concentration p inside of the semiconductor of thickness d

$$0 = -\frac{1}{q} \frac{\partial j_h}{\partial x} + G_h(x) - R_h(x). \quad (22)$$

We consider the generation rate of charge carriers from the simple Lambert-Beer law $G_h(x) = \alpha P e^{-\alpha x}$, where $P = \int_{\lambda_{min}}^{\lambda_g} \Phi(\lambda) d\lambda$ is number of photons with energy above $E_g = \frac{hc}{\lambda_g}$ which are absorbed in the semiconductor, $\Phi(\lambda)$ is the spectral photon flux of standard AM15G spectrum with intensity 100 mW/cm²,²⁵ α is the absorption coefficient of the semiconductor. The hole current density j_h is expressed using the analytical solution of Poisson's equation

$$j_h = -qD_h \frac{\partial p}{\partial x} - q\mu_h p \frac{\partial \phi_a}{\partial x}, \quad (23)$$

where $\mu_h = \frac{qD_h}{k_B T}$ is the hole mobility, and D_h is the hole diffusion constant. A direct band-to-band nonlinear recombination is assumed

$$R_h = \frac{1}{N_D \tau_h} (n_{dark} p - n_i^2). \quad (24)$$

We assume that charge transfer under illumination occurs exclusively from the valence band to the electrolyte. We do not include charge transfer from surface states in the current analysis. The transfer current density of valence band holes at the SEI is described by a first-order approximation²⁶

$$j_h(0) = -q k_{trh} (p(0) - p_{dark}(0)), \quad (25)$$

where k_{trh} is the rate constant for hole transfer, and a linear dependence on the deviation of the interfacial hole concentration $p(0)$ from its dark value $p_{dark}(0)$ at the interface is assumed. Since the thickness of the semiconductor is in the order of the penetration length of light α^{-1} for the hematite parameters listed in 1, we consider the hole current at the back contact of the semicon-

ductor to depend on a surface recombination velocity r_s

$$j_h(d) = +q r_s (p(d) - p_{0i}). \quad (26)$$

We use $r_s = 10^5$ m/s for numerical calculations throughout this article.¹² In order to obtain convergence of the numerical solution procedure, the continuity equation was solved in a non-dimensional form after applying the usual normalization of the variables of the drift-diffusion equations.²⁷

The quasi-Fermi energies E_{Fn}, E_{Fp} under the influence of an electrostatic potential $\phi(x)$ are calculated by the Boltzmann distribution

$$n(x) = N_C \exp\left(-\frac{E_c(x) - E_{Fn}}{k_B T}\right), \quad (27)$$

$$p(x) = N_V \exp\left(-\frac{E_{Fp} - E_v(x)}{k_B T}\right). \quad (28)$$

Results We numerically solved the hole (electron) continuity equation Eq. 22 for a n-type (p-type) semiconductor by using the depletion region approximation of the electrostatic potential Eq. 21. Results for n-type Fe_2O_3 and p-type Cu_2O are presented in the following. If not otherwise stated, we assume $\phi_{el} = 0$ V and $V_H^{fb} = V_{H0} = V_H$ in the following.

Fe_2O_3 The charge carrier concentration profiles calculated from the model are plotted in 2. In the dark, the SCR is depleted of electrons and the concentrations of holes is increased with respect to the bulk hole concentration. For increasing $V_{r,RHE}$, the dark electron concentration at the SEI $n_{dark}(0)$ decreases until it is smaller than the dark hole concentration at the SEI $p_{dark}(0)$, leading to an inversion layer characterized by a larger concentration of holes (minorities) than electrons (majorities) in the SCR. Corresponding value of $V_{sc}^{inv} = V_{th} \ln\left(\frac{N_D}{n_i}\right) = 0.88$ V and thus $V_{r,RHE}^{inv} = 1.4$ V are obtained. Therefore, a more detailed future model should take into account the electron continuity equation instead of assuming that the electron concentration upon illumination is equal to the electron concentration in the dark.

Upon illumination, the concentration of electrons is equal to the dark electron concentration.

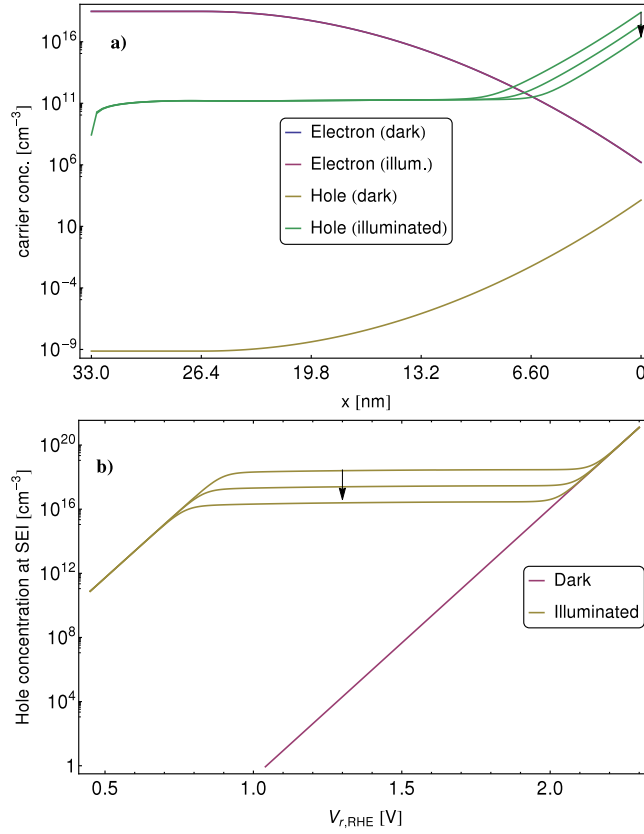
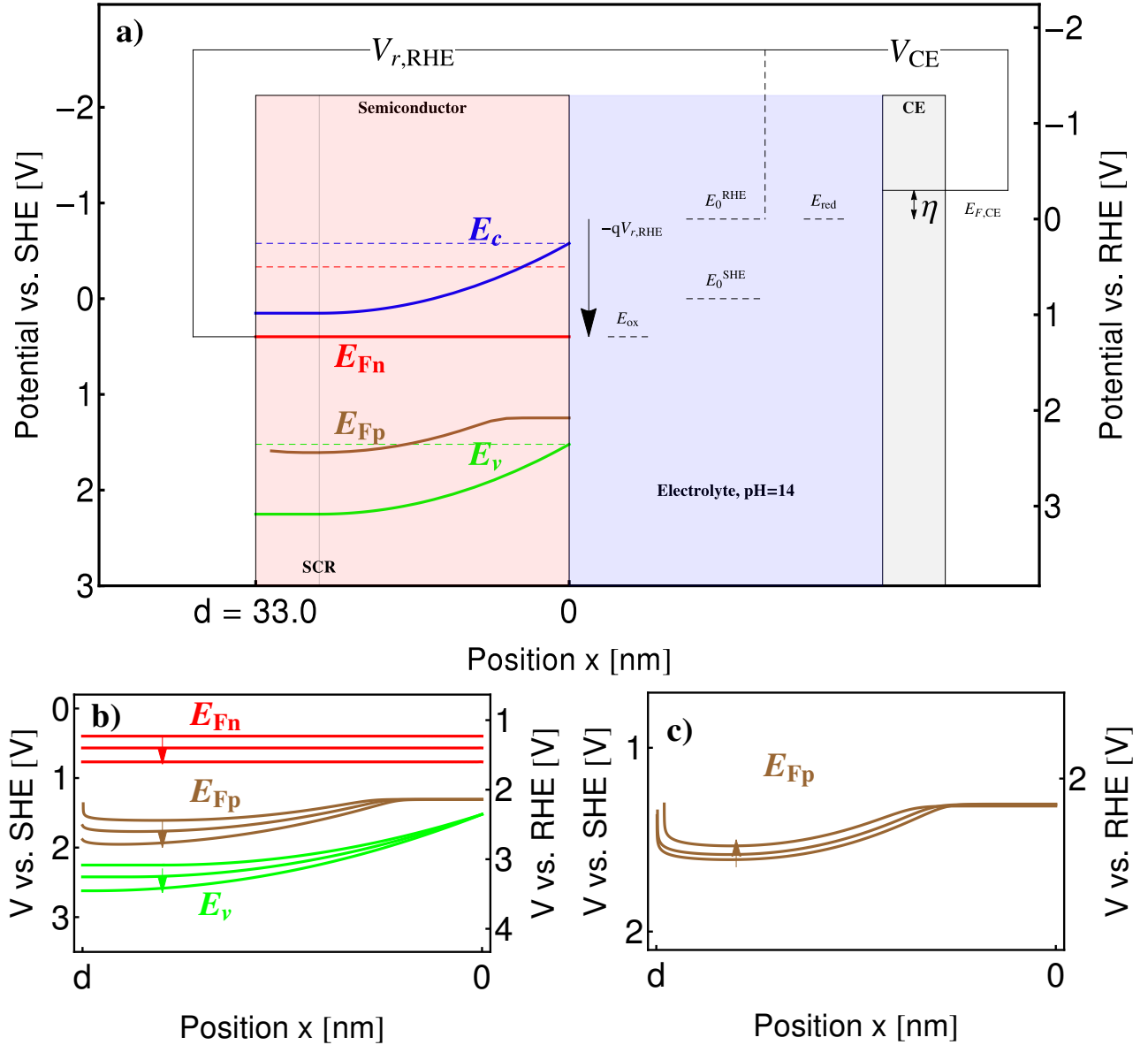


Figure 2: a) The simulated charge carrier concentrations in the semiconductor are shown for a measurable voltage of $V_{r,RHE}=1.23$ V. b) Hole concentration at SEI as a function of $V_{r,RHE}$. Direction of arrows mean increasing $k_{trh}=10^{-4}, 10^{-3}, 10^{-2}$ m/s. Model parameters for hematite from 1 were used.

Less holes are accumulated near the SEI for increasing rate constant k_{trh} (faster charge transfer), 2. For large $V_{r,RHE}$ (>2.0 V), the hole concentration upon illumination near the SEI approaches the hole concentration in the dark, 2b. At the back contact, the hole concentration follows from solution of continuity equation and boundary condition eq. 26.

The energy band diagram is shown for a three-electrode setup in 3. A measurable voltage of $V_{r,RHE} = 1.23$ V is assumed, which is the standard voltage used for comparison of different PEC electrodes.^{28,29} The measurable voltage $V_{r,RHE}$ is indicated in 3a) with an arrow on the energy scale, $-qV_{r,RHE}$. This is also explained in our previous work.²⁴ The band edges of the semiconductor $E_c(x), E_v(x)$ for flatband condition ($V_{r,RHE} = V_{fb,RHE}$) are shown as dashed lines, whereas those away from flatband condition ($V_{r,RHE} \neq V_{fb,RHE}$) are shown as solid lines. Band positions at flatband conditions for hematite agree well with values reported for example for $pH = 1$ ^{30,31} and $pH = 14$.³² An upward band bending of the semiconductor is present if $V_{r,RHE}$ V is more positive than $V_{fb,RHE}$, see ??. Band edges are pinned at the SEI by default (since we assume $V_H = V_H^{fb}$), but we allow for modification of surface conditions by changing the value of V_H in our interactive band diagram software.²¹

The number of photogenerated electrons is small compared to the donor concentration, and thus illumination does not change the electron concentration. Therefore, the electron quasi-Fermi level E_{Fn} is also constant across the semiconductor, eq. 27, and $E_{Fn} = E_{Fn,b}$. The position of E_{Fn} relative to E_0^{RHE} in the energy diagram is given by arrow $-qV_{r,RHE}$, eq. ??. In contrast, the hole concentration is determined mainly by photogenerated holes, which are redistributed in the semiconductor according to the continuity equation Eq. 22. Since $E_v(0)$ is more positive than E_{ox} , a transfer of holes from the valence band can thermodynamically oxidize the electrolyte species. An external wire electrically connects the semiconductor to the metal counter electrode (CE) through a potentiostat. The counter electrode Fermi level $E_{F,CE}$ is automatically adjusted by applying a voltage V_{CE} above the water reduction energy E_{red} (including the electrochemical overpotential η) by the potentiostat to enable hydrogen evolution at the counter electrode. The counter electrode is shown in the energy diagram only to completely describe a three-electrode setup and we ignore its



polarization in the following.³³ In the electrolyte, we plot two reference electrode energies E_0^{SHE} and E_0^{RHE} , standard water reduction and oxidation energy E_{red} (0 eV vs RHE) and E_{ox} (1.23 eV vs RHE). Note that the relation of E_{red} and E_{ox} to E_{redox} depends on the concentrations (activities) of oxidizing and reducing species in the solution.³⁴

The energy band diagram in the semiconductor for different values of the measurable voltage $V_{r,RHE}$ is plotted in 3b). For increasing $V_{r,RHE}$ the band bending increases and the electron quasi-Fermi level E_{Fn} shifts down on the RHE scale. Interestingly, the hole quasi-Fermi level $E_{Fp}(0)$ at the SEI remains nearly constant for increasing $V_{r,RHE}$ (see Figure S1 in Supporting Information) and thus the splitting of the quasi-Fermi levels (photovoltage) approaches zero. In the neutral region $w < x < d$, the hole quasi-Fermi level $E_{Fp}(x)$ is more negative for increasing $V_{r,RHE}$ and the photovoltage is nearly constant. When the hole diffusion length $L_h = \sqrt{D_h \tau_h}$ is increased, the flat region of the hole quasi-Fermi level E_{Fp} near the SEI is enlarged, 3c), and the hole concentration in the neutral region decreases (see Figure S2 in Supporting Information).

We simulated current-voltage curves with our numerical model $j_h(0)$ (eq. 25) and compared the results with published models of Gartner⁸ and Reichmann,¹⁰ 4. According to Gartner, the minority charge carrier concentration is calculated from the diffusion equation, neglecting recombination in the SCR and assuming that every hole in SCR contributes to the photocurrent. Photocurrent density of Gartner is

$$j_G = eP \left(1 - \frac{e^{-\alpha w}}{1 + \alpha L_h} \right). \quad (29)$$

Therefore, j_G overestimates the minority carrier photocurrent in comparison to our numerical model $j_h(0)$. Recombination in the SCR by Sah-Noyce-Shockley formalism was incorporated into the model by Reichmann¹⁰ with resulting photocurrent j_R (the detailed expression is given in the Supporting Information). For small $V_{r,RHE}$, j_R is much smaller than j_G because the SCR recombination loss is included in j_R . The onset of the photocurrent calculated by Reichmann j_R starts when $\gamma = \frac{j_s e^{-\frac{V_{app}}{V_{th}}}}{q k_{trh} p_{dark}(0)} \approx 1$ (j_s is the saturation current density as defined in the SI). Therefore, if we consider faster charge transfer kinetics (larger k_{trh}), we need a smaller value of the onset potential $V_{r,RHE}$ (and thus V_{app}) to obtain a similar value $\gamma \approx 1$. For increasing $V_{r,RHE}$, j_R approaches

j_G because the SCR recombination becomes negligible in j_R ,¹⁰ but the numerical photocurrent $j_h(0)$ is smaller than j_G since SCR recombination is included in $j_h(0)$. The numerical photocurrent $j_h(0)$ onsets when $V_{r,RHE}$ is more positive than $V_{fb,RHE}$ and it is larger than j_R for small $V_{r,RHE}$. Increasing the rate constant k_{trh} represents a faster exchange rate of holes with the solution. This also shifts the numerical j-V curve to the left as predicted by the Reichmann model, decreasing the onset potential of the photocurrent.

Measured current-voltage curve for nanostructured Fe_2O_3 electrode with IrO_2 catalyst³⁵ is compared with the prediction from our model on 4. The onset voltage of measured photocurrent $\approx 0.8 \text{ V}_{RHE}$ is reproduced with numerical photocurrent with $k_{trh} = 10^{-4} \text{ m/s}$. However, the slope of measured photocurrent and its value 4.3 mA/cm^2 at $1.5 \text{ V}_{r,RHE}$ is smaller than the slope of numerical photocurrent and its value 3.8 mA/cm^2 at $1.5 \text{ V}_{r,RHE}$. These differences point out that we cannot verify our model description by comparing the current-voltage curves alone, because the kinetic effects cannot be distinguished in the current-voltage response. Comparison of the model predictions with impedance spectroscopy³⁶ measurements is needed to verify the model.

We checked that the maximum photocurrent obtainable from the hematite electrode based purely on the number of absorbed photons is $qP = 12.5 \text{ mA/cm}^2$ for AM15G illumination. This value is also obtained for the Gartner photocurrent eq. ?? when the bracket term is close to one and also for the Reichmann photocurrent (which recovers the Gartner photocurrent in regime of large voltages). The plateau of numerical photocurrent $j_h(0)$ cannot be computed here, because our model cannot be used to predict photocurrents at voltages higher than $V_{r,RHE} > V_{r,RHE}^{inv}$. At such voltages inversion layer is formed as described in the previous text and this would need degenerate statistics to be included in the model.

Cu₂O We also applied our model to simulate p-type semiconductors for photocathodes. Appropriate changes in the equations were introduced, resulting from doping with acceptors rather than donors. Cuprous oxide (Cu_2O) is an abundant and promising material for PEC photocathodes. The main issue with Cu_2O is its limited stability in water, which is currently being addressed with

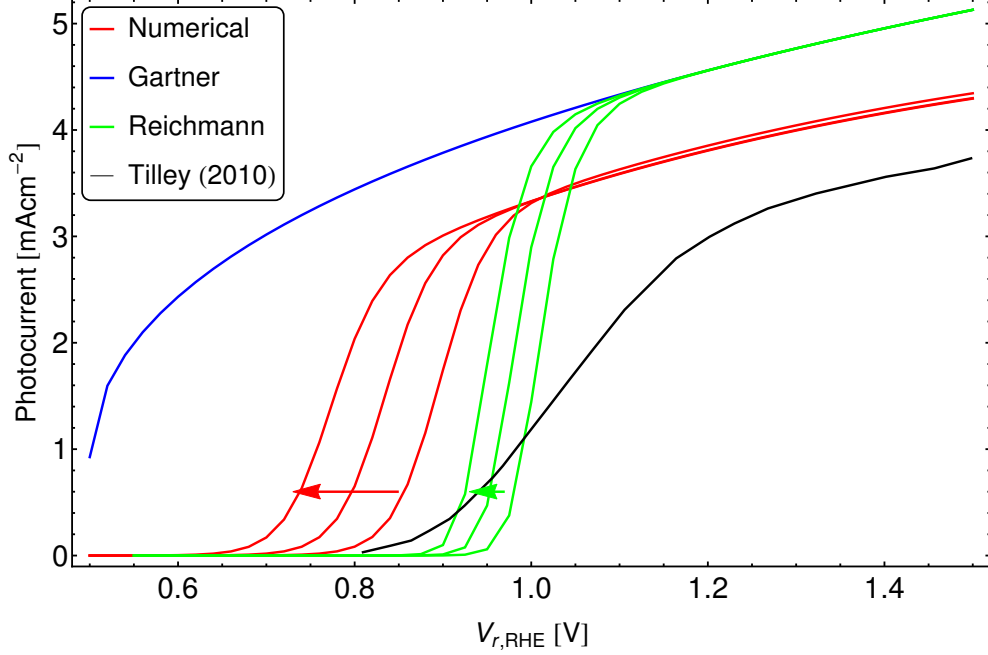


Figure 4: Current-voltage curves for $k_{trh} = 10^{-4}, 10^{-3}, 10^{-2}$ m/s (in direction of arrows) from our numerical model, Gartner model and Reichmann model for n-doped hematite and other material parameters listed in 1.

stabilizing overlayers.^{37–39} A downward band-bending occurs when $V_{r,RHE}$ is more negative than $V_{fb,RHE}$. This leads to a drift of electrons to the electrolyte, 5. Upon illumination, the hole concentration is assumed to remain equal to the dark hole concentration. The electron concentration is calculated from the electron continuity equation. Electrons are accumulated near the SEI where they reduce water to H_2 with a rate constant k_{tre} .

In the case of p-type Cu_2O , the majority carriers are holes, and thus the counter electrode carries out the oxidation reaction (including the associated overpotential η). Although the electron quasi-Fermi level E_{Fn} is negative with respect to E_{red} making it suitable for hydrogen evolution, 5, corrosion prevents hydrogen evolution in the experiment unless the Cu_2O is protected by overlayers.³⁷ So far, our model does not consider corrosion; here we aimed at showing the general energetic configuration of a p-type PEC photoelectrode.

Conclusion We presented a physical model for minority charge carrier transport in semiconductor PEC electrodes in contact with an electrolyte. Direct charge transfer to the electrolyte from

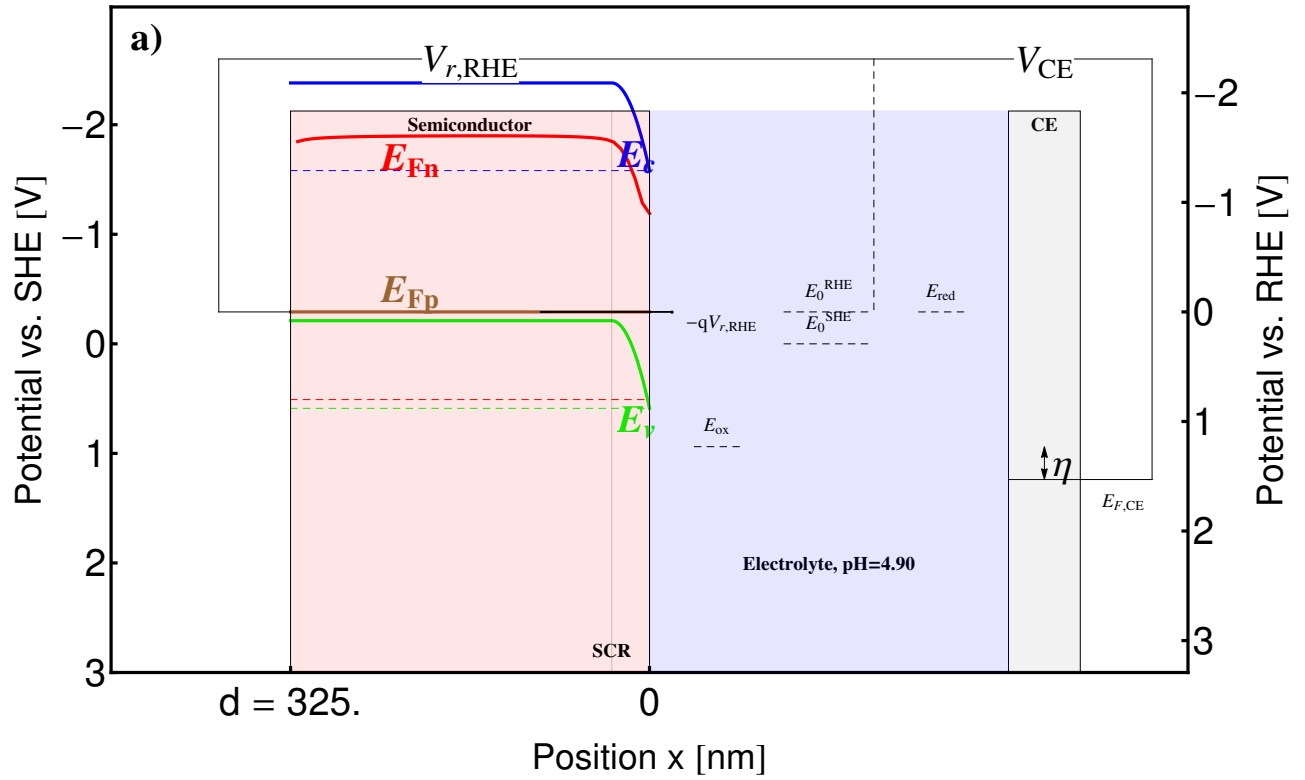


Figure 5: Energy band diagram for p-doped Cu_2O , $k_{\text{tre}} = 10$ m/s and $V_{r,\text{RHE}} = 0$ V (hence the voltage arrow is not visible in the diagram). The material parameters are listed in 1. The interactive version of this figure can be accessed at <http://icp.zhaw.ch/PEC>.

valence or conduction band, band-to-band recombination and Lambert-Beer optical generation were assumed. A numerical solution of the model equations allows us to calculate the minority carrier concentration and the quasi-Fermi level. A resulting energy band diagram of a PEC cell accounts for the potential drop in the Helmholtz layer and it is capable of modeling both band edge pinning and unpinning. Comparison of the numerically obtained photocurrent with analytical results and measurement reveals need for verification of the model with spectroscopic measurements. Our model was implemented in an interactive software that can be freely accessed online.²¹ All presented results of this article can be reproduced with this software and we invite all members of the research community to use it while designing PEC cells. We are currently working on an extension of our model to a fully coupled drift-diffusion model with surface states. Such photoelectrode models need to accompany the experimental studies to suppress recombination losses (e.g. by surface passivation) and enhance charge transfer (e.g. by catalysis), the two major issues for efficient metal oxide photoelectrodes.⁴⁰

Acknowledgement

We thank F.T. Abdi, H. J. Lewerenz, G. Schlichthoerl and B. Klahr for fruitful discussions. Financial support by the Swiss Federal Office of Energy (PECHouse2 project, contract number SI/500090-02) is gratefully acknowledged.

References

- (1) Lewis, N. S.; Nocera, D. G. *Proceedings of the National Academy of Sciences* **2006**, *103*, 15729–15735.
- (2) Schiermeier, Q. *Nature* **2013**, *496*, 156–158.
- (3) Khaselev, O.; Turner, J. A. *Science* **1998**, *280*, 425–427.
- (4) van de Krol, R.; Liang, Y. *CHIMIA International Journal for Chemistry* **2013**, *67*, 168–171.

Table 1: Material parameters of semiconductors used in the calculations.

Symbol	Fe ₂ O ₃ ⁴¹	Cu ₂ O ^{38,42}	Description
N_D [cm ⁻³]	$2.91 \cdot 10^{18}$	0	Donor concentration
N_A [cm ⁻³]	0	$5 \cdot 10^{17}$	Acceptor concentration
$V_{fb,RHE}$ [V]	+0.5	+0.8	Flatband potential
χ [eV]	+4.78 ^{43,44}	+4.22 ⁴³	Electron affinity
N_C [cm ⁻³]	$4 \cdot 10^{22}$ ^{45,46}	$1.1 \cdot 10^{19}$	Density of states of CB
N_V [cm ⁻³]	$1 \cdot 10^{22}$	$1.1 \cdot 10^{19}$	Density of states of VB
ϵ_r	32 [?]	6.6	Relative permittivity
E_g [eV]	2.1	2.17	Bandgap energy
d [nm]	33	325	Thickness of semiconductor
τ_e [ns]	-	0.25	Electron lifetime
τ_h [ns]	0.048 ⁴⁷	-	Hole lifetime
L_e [nm]	-	40	Electron diffusion length
L_h [nm]	5 ⁷	-	Hole diffusion length
α [cm ⁻¹]	$1.5 \cdot 10^5$	$1.3 \cdot 10^4$	Absorption coefficient
pH	14	4.9	pH value of the electrolyte

- (5) Sivula, K. *CHIMIA International Journal for Chemistry* **2013**, 67, 155–161.
- (6) Abdi, F. F.; Han, L.; Smets, A. H. M.; Zeman, M.; Dam, B.; van de Krol, R. *Nature Communications* **2013**, 4, year.
- (7) Krol, R. V. D.; Grätzel, M. *Photoelectrochemical Hydrogen Production*; Springer, 2011.
- (8) Gärtner, W. W. *Physical Review* **1959**, 116, 84–87.
- (9) Wilson, R. H. *Journal of Applied Physics* **1977**, 48, 4292–4297.
- (10) Reichman, J. *Applied Physics Letters* **1980**, 36, 574–577.
- (11) Andrade, L.; Lopes, T.; Ribeiro, H. A.; Mendes, A. *International Journal of Hydrogen Energy* **2011**, 36, 175–188.
- (12) Foley, J. M.; Price, M. J.; Feldblyum, J. I.; Maldonado, S. *Energy & Environmental Science* **2012**, 5, 5203–5220.
- (13) Peter, L.; Li, J.; Peat, R. *Journal of Electroanalytical Chemistry and Interfacial Electrochemistry* **1984**, 165, 29–40.

- (14) Klahr, B.; Gimenez, S.; Fabregat-Santiago, F.; Hamann, T.; Bisquert, J. *J. Am. Chem. Soc.* **2012**, *134*, 4294–4302.
- (15) Bertoluzzi, L.; Bisquert, J. *The Journal of Physical Chemistry Letters* **2012**, 2517–2522.
- (16) Carver, C.; Ulissi, Z.; Ong, C.; Dennison, S.; Kelsall, G.; Hellgardt, K. *International Journal of Hydrogen Energy* **2012**, *37*, 2911–2923.
- (17) Haussener, S.; Hu, S.; Xiang, C.; Weber, A. Z.; Lewis, N. *Energy & Environmental Science* **2013**.
- (18) Salvador, P. *The Journal of Physical Chemistry B* **2001**, *105*, 6128–6141.
- (19) Memming, R. *Semiconductor Electrochemistry*; John Wiley & Sons, 2008.
- (20) Peter, L. M. *Journal of Solid State Electrochemistry* **2013**, *17*, 315–326.
- (21) Cendula, P. *The model is available freely on the internet.* <http://icp.zhaw.ch/PEC>.
- (22) Dotan, H.; Sivula, K.; Grätzel, M.; Rothschild, A.; Warren, S. C. *Energy & Environmental Science* **2011**, *4*, 958.
- (23) Klahr, B. M.; Hamann, T. W. *Applied Physics Letters* **2011**, *99*, 063508–063508–3.
- (24) Bisquert, J.; Cendula, P.; Bertoluzzi, L.; Gimenez, S. *The Journal of Physical Chemistry Letters* **2013**, 205–207.
- (25) NREL, *Solar Spectral Irradiance: Air Mass 1.5, downloaded March 2012*, 2012. <http://redc.nrel.gov/solar/spectra/am1.5/>.
- (26) Tan, M. X.; Laibinis, P. E.; Nguyen, S. T.; Kesselman, J. M.; Stanton, C. E.; Lewis, N. S. Principles and Applications of Semiconductor Photoelectrochemistry. In *Progress in Inorganic Chemistry*; Karlin, K. D., Ed.; John Wiley & Sons, Inc., 1994; pp 21–144.

- (27) Markowich, P. A.; Ringhofer, C. A.; Schmeiser, C. *Semiconductor equations*; Springer-Verlag New York, Inc.: New York, NY, USA, 1990.
- (28) Kay, A.; Cesar, I.; Grätzel, M. *J. Am. Chem. Soc.* **2006**, *128*, 15714–15721.
- (29) Chen, Z.; Deutsch, T. G.; Dinh, H. N.; Domen, K.; Emery, K.; Forman, A. J.; Gaillard, N.; Garland, R.; Heske, C.; Jaramillo, T. F.; Kleiman-Shwarsstein, A.; Miller, E.; Takanabe, K.; Turner, J. Efficiency Definitions in the Field of PEC. In *Photoelectrochemical Water Splitting*; SpringerBriefs in Energy; Springer New York, 2013; pp 7–16.
- (30) Nozik, A. J. *Annual Review of Physical Chemistry* **1978**, *29*, 189–222.
- (31) Grätzel, M. *Nature* **2001**, *414*, 338–344.
- (32) Krol, R. v. d.; Liang, Y.; Schoonman, J. *J. Mater. Chem.* **2008**, *18*, 2311–2320.
- (33) Hodes, G. *The Journal of Physical Chemistry Letters* **2012**, *3*, 1208–1213.
- (34) Morrison, S. R. *Electrochemistry at semiconductor and oxidized metal electrodes*; Plenum Press, 1980.
- (35) Tilley, S. D.; Cornuz, M.; Sivula, K.; Grätzel, M. *Angewandte Chemie* **2010**, *122*, 6549–6552.
- (36) Klahr, B.; Gimenez, S.; Fabregat-Santiago, F.; Bisquert, J.; Hamann, T. W. *Energy & Environmental Science* **2012**, *5*, 7626–7636.
- (37) Paracchino, A.; Laporte, V.; Sivula, K.; Grätzel, M.; Thimsen, E. *Nat Mater* **2011**, *10*, 456–461.
- (38) Paracchino, A.; Mathews, N.; Hisatomi, T.; Stefik, M.; Tilley, S. D.; Grätzel, M. *Energy & Environmental Science* **2012**, *5*, 8673.
- (39) Tilley, S. D.; Schreier, M.; Azevedo, J.; Stefik, M.; Graetzel, M. *Advanced Functional Materials* **2013**, n/a–n/a.

- (40) Sivula, K. *The Journal of Physical Chemistry Letters* **2013**, *4*, 1624–1633.
- (41) Upul Wijayantha, K.; Saremi-Yarahmadi, S.; Peter, L. M. *Physical Chemistry Chemical Physics* **2011**, *13*, 5264.
- (42) Paracchino, A.; Brauer, J. C.; Moser, J.-E.; Thimsen, E.; Graetzel, M. *The Journal of Physical Chemistry C* **2012**, *116*, 7341–7350.
- (43) Xu, Y.; Schoonen, M. A. A. *American Mineralogist* **2000**, *85*, 543–556.
- (44) Niu, M.; Huang, F.; Cui, L.; Huang, P.; Yu, Y.; Wang, Y. *ACS Nano* **2010**, *4*, 681–688.
- (45) Morin, F. J. *Physical Review* **1954**, *93*, 1195–1199.
- (46) Cesar, I.; Sivula, K.; Kay, A.; Zboril, R.; Grätzel, M. *J. Phys. Chem. C* **2008**, *113*, 772–782.
- (47) Bosman, A.; van Daal, H. *Advances in Physics* **1970**, *19*, 1–117.

Table 2: Table of symbols and abbreviations. Symbols for material parameters are defined in 1.

Symbol	Unit	Description
CE		Counter electrode
LVL		Local vacuum level
PEC		Photoelectrochemical
SCR		Space-charge region
SEI		Semiconductor-electrolyte interface
SHE		Standard hydrogen electrode
SI		Supporting information
RHE		Reversible hydrogen electrode
<i>Subscript i</i>		Quantity in the isolated semiconductor before contact to an electrolyte
<i>Subscript b</i>		Quantity in the semiconductor bulk
<i>Subscript s</i>		Quantity at the SEI
k_B	eV/K	Boltzmann constant ($8.6 \cdot 10^{-5}$ eV/K)
T	K	Temperature (300 K)
q	C	Elementary charge ($1.6 \cdot 10^{-19}$ C)
V_{th}	V	Thermal voltage (25.9 mV)
h	J·s	Planck's constant ($6.62607 \cdot 10^{-34}$ J·s)
c	m/s	Speed of light in vacuum (299792458 m/s)
V_r	V	Measurable voltage with respect to SHE reference electrode
$V_{r,RHE}$	V	Measurable voltage with respect to RHE
$V_{r,RHE}^{inv}$	V	Measurable voltage with respect to RHE when the inversion layer starts to form
V_{fb}	V	Flatband voltage with respect to SHE
$V_{fb,RHE}$	V	Flatband voltage with respect to RHE
V_{app}	V	Applied voltage to the semiconductor with respect to the dark equilibrium (unbiased)
V_H	V	Potential (voltage) drop across the Helmholtz layer in the dark
V_H^{fb}	V	Potential (voltage) drop across the Helmholtz layer at flatband situation in the dark
V_{H0}	V	Potential (voltage) drop across the Helmholtz layer in the dark equilibrium
V_{sc}	V	Potential (voltage) drop across the semiconductor
V_{bi}	V	Built-in voltage of semiconductor/liquid junction
V_{CE}	V	Voltage between the reference electrode and counterelectrode
η	V	Electrochemical overpotential at the CE
E_{vac}	eV	Energy of the local vacuum level
E_0^{SHE}	eV	Energy of the SHE with respect to vacuum level of the electron (-4.44 eV)
E_0^{RHE}	eV	Energy of the RHE with respect to vacuum level of the electron
E_{redox}	eV	Fermi level of the electrolyte species (redox level)
E_{red}	eV	Standard water reduction energy
E_{ox}	eV	Standard water oxidation energy
E_{F0}	eV	Equilibrium Fermi level in the semiconductor (dark)
$E_{c,0i}$	eV	Conduction band edge in the isolated semiconductor before contact to an electrolyte
$E_{F,0i}$	eV	Fermi level in the isolated semiconductor before contact to an electrolyte
E_{Fn}, E_{Fp}	eV	Quasi-Fermi energy of electrons and holes
$E_{Fn,b}$	eV	Quasi-Fermi energy of electrons at the back contact
E_c	eV	Conduction band edge in the semiconductor
E_v	eV	Valence band edge in the semiconductor
$E_{F,CE}$	eV	Fermi level of the CE
ζ_{nb}	eV	The difference between the semiconductor conduction band energy and the electron Fermi level
ϕ	V	Local electrostatic potential
ϕ_a	V	Approximate solution for local electrostatic potential
ϕ_{el}	V	Local electrostatic potential of the electrolyte
ϕ_s	V	Local electrostatic potential at SEI
ϕ_b	V	Local electrostatic potential in the semiconductor bulk

Table 2 continued.

Symbol	Unit	Description
n_i	m^{-3}	Intrinsic carrier concentration in the bulk of semiconductor
n_{0i}, p_{0i}	m^{-3}	Equilibrium concentration of electrons and holes in the bulk of isolated semiconductor
n_{dark}, p_{dark}	m^{-3}	Dark concentration of electrons and holes
n, p	m^{-3}	Concentration of electrons and holes
w	m	Width of the space-charge region in the semiconductor
j_h	A/m^2	Hole current density
j_G	A/m^2	Current density calculated by Gartner ⁸
j_R	A/m^2	Current density calculated by Reichmann ¹⁰
j_s	A/m^2	Saturation current density
G_h, R_h	$\text{m}^{-3}\text{s}^{-1}$	Generation and recombination rate of holes
P	$\text{m}^{-2}\text{s}^{-1}$	Number of photons absorbed in the semiconductor from AM15G spectrum
Φ	$\text{m}^{-3}\text{s}^{-1}$	Spectral photon flux of AM15G spectrum
μ_h	$\text{m}^2\text{V}^{-1}\text{s}^{-1}$	Mobility of holes
D_h	m^2s^{-1}	Diffusion constant of holes
k_{trh}	ms^{-1}	Rate constant for charge transfer of VB holes to electrolyte
λ_g	m	Wavelength below which semiconductor absorbs photons
r_s	ms^{-1}	Back contact surface recombination velocity